Material and Methods

Simulation methods

We used our previously described simulation platform (Deinum et al., 2012) to simulate changes in auxin transport in root segments representing the susceptible zone of legume roots. Inside cells and within the apoplast, auxin moves by diffusion with diffusion constants 300 $\mu m^2\ s^{-1}$ and 44 $\mu m^2\ s^{-1}$, respectively. Auxin transport over membranes is modeled using effective permeabilities. This results in an outward flux of $J_{mem} = C_{cell}\ P_{eff} - C_{wall}\ P_{inf}$, with negative values indicating a net inward flux. In this, C_{cell} and C_{wall} are the concentrations in the pixels on either side of the membrane, P_{eff} is the local effective efflux permeability, which starts at one of three levels ("high" = 20 $\mu m\ s^{-1}$, "low" = 5 $\mu m\ s^{-1}$, or "bg" (background level) = 1 $\mu m\ s^{-1}$ as shown in fig. 3B), and P_{inf} = 20 $\mu m\ s^{-1}$ the effective influx permeability, as shown in figure 13A.

The PIN layout of these root segments is derived from the model of (Laskowski et al., 2008), which is based on their experimental observations in Arabidopsis, with cell sizes and number of cortical layers adapted to the Medicago geometry. Individual cells are 100 µm long and 20 µm (cortex) or 10 µm (all others) wide.

In the middle of the segment we have indicated a five cell long block of cells, comprising epidermis to pericycle on one side of the root, which we call the "controlled area". At T = 0 we reduce all P_{eff} parameters in the controlled area by a factor 10. Using larger factors did not affect the qualitative behaviour of the model, i.e., any of the effects described in the main text. It only resulted in larger absolute increases of the auxin concentration and corresponding increases of the time to reach the new steady state concentration (not shown).

The full segments are 28 cells long to avoid boundary effects near the controlled area. For further details and references, see (Deinum et al., 2012). Because we focus on early events we used a smaller integration time step of 0.1 second.

Deinum, E. E., Geurts, R., Bisseling, T. and Mulder, B. M. (2012). Modeling a cortical auxin maximum for nodulation: different signatures of potential strategies. *Front Plant Sci.* **3**, 96.

Laskowski, M., Grieneisen, V. A., Hofhuis, H., Hove, C. A. t., Hogeweg, P., Maree, A. F. M. and Scheres, B. (2008). Root system architecture from coupling cell shape to auxin transport. *PLoS Biology* **6**, 2721-2735.

Constructs

The *AtCASP1::GUS* construct is described in Roppolo et al., 2011. For *MtENOD40::GUS* and *AtSCR::GUS* constructs, DNA fragments of putative promoters were amplified from *M. truncatula* and *A. thaliana* genomic DNA respectively using primer combinations listed in Table S1 and **Phusion™ High-Fidelity DNA Polymerase** (Finnzymes).Then, the Gateway® technology (Invitrogen) was used to create genetic promoter-GUS constructs (Karimi et al., 2002). For *MtENOD40::GUS*, the pENTR™/D-TOPO® Cloning Kits (Invitrogen) was used to create entry clones. The entry vector was recombined into Gateway®-compatible binary vector pKGW-RR, that contains GUS reporter gene and *AtUBQ10::DsRED1* as a selection marker (Limpens et al., 2004), by using Gateway® LR Clonase® II enzyme mix (Invitrogen). For *AtSCR::GUS*, the *AtSCR* DNA fragment was introduced into Gateway® donor vector pENTR4-1, GUS reporter gene into pENTR1-2 and 35S CaMV terminator into pENTR2-3, using Gateway® BP Clonase® II enzyme mix. These entry vectors were recombined into Gateway®-compatible binary vector pKGW-RR-MGW, that contains *AtUBQ10::DsRED1* as a selection marker using Gateway® LR Clonase® II Plus enzyme mix (Invitrogen).

Karimi, M., Inze, D. and Depicker, A. (2002). GATEWAY^{TM} vectors for *Agrobacterium*-mediated plant transformation. *Trends Plant Sci.* **7**, 193-195.
Limpens, E., Ramos, J., Franken, C., Raz, V., Compaan, B., Franssen, H., Bisseling, T. and Geurts, R. (2004). RNA interference in *Agrobacterium rhizogenes*-transformed roots of *Arabidopsis* and *Medicago truncatula*. *J. Exp. Bot.* **55**, 983-992.
Roppolo, D., De Rybel, B., Tendon, V. D., Pfister, A., Alassimone, J., Vermeer, J. E., Yamazaki, M., Stierhof, Y. D., Beeckman, T. and Geldner, N. (2011). A novel protein family mediates Casparian strip formation in the endodermis. *Nature* **473**, 380-383.

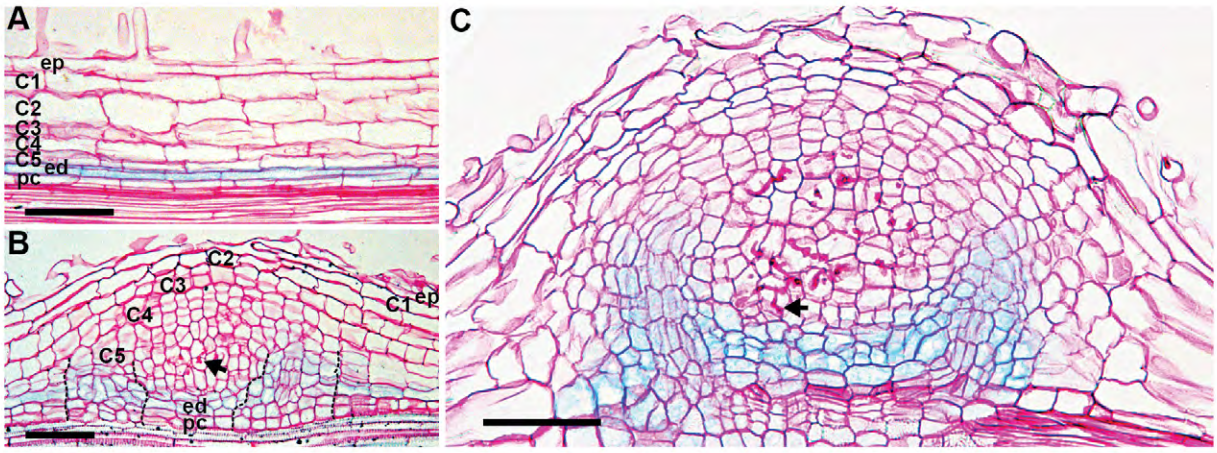

Fig. S1. *AtSCR::GUS* is expressed in endodermis (A) and cells derived from endodermis (B) and these cells are not infected by rhizobium (B-C) (Infection threads are indicated by arrows).

In B, cells at the periphery region (indicated in between black lines) will differentiate into nodule parenchyma include vascular bundles and endodermis.

Bars, 75 μm.

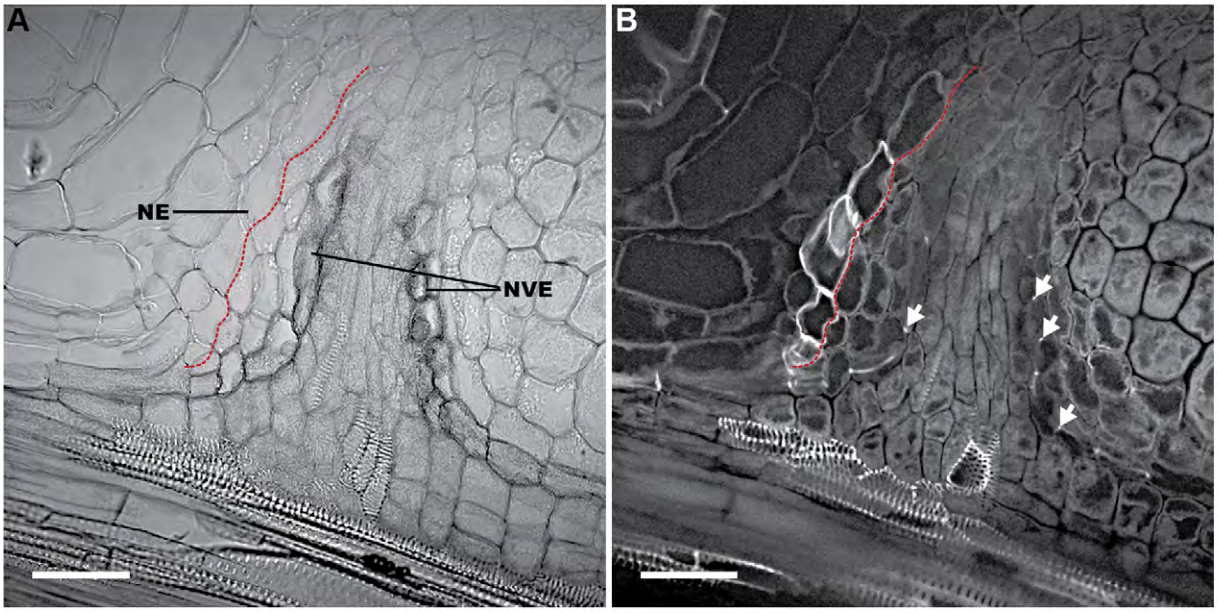

Fig. S2. Casparian strips are present in cells where *AtCASP1::GUS* is expressed.

Split channels of Fig. 5D. (A) *AtCASP1::GUS* is expressed in NVE but not in NE; (B) Casparian strips (arrows) are present in NVE but not in NE.

Bars, 50 µm.

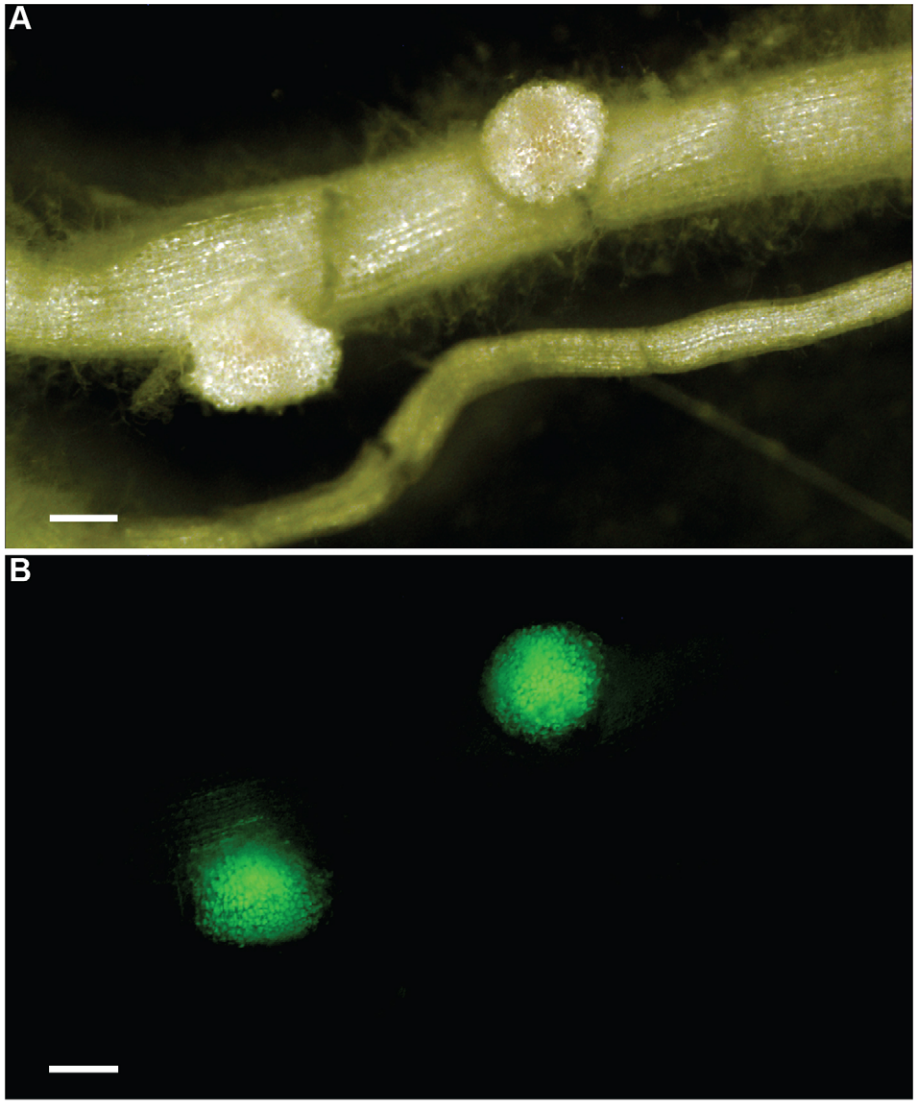

Fig. S3. *Sinorhizobium meliloti* strain 2011 expresses nifH::GFP in *nf-ya1-1* nodules.

Bars, 250 μm.

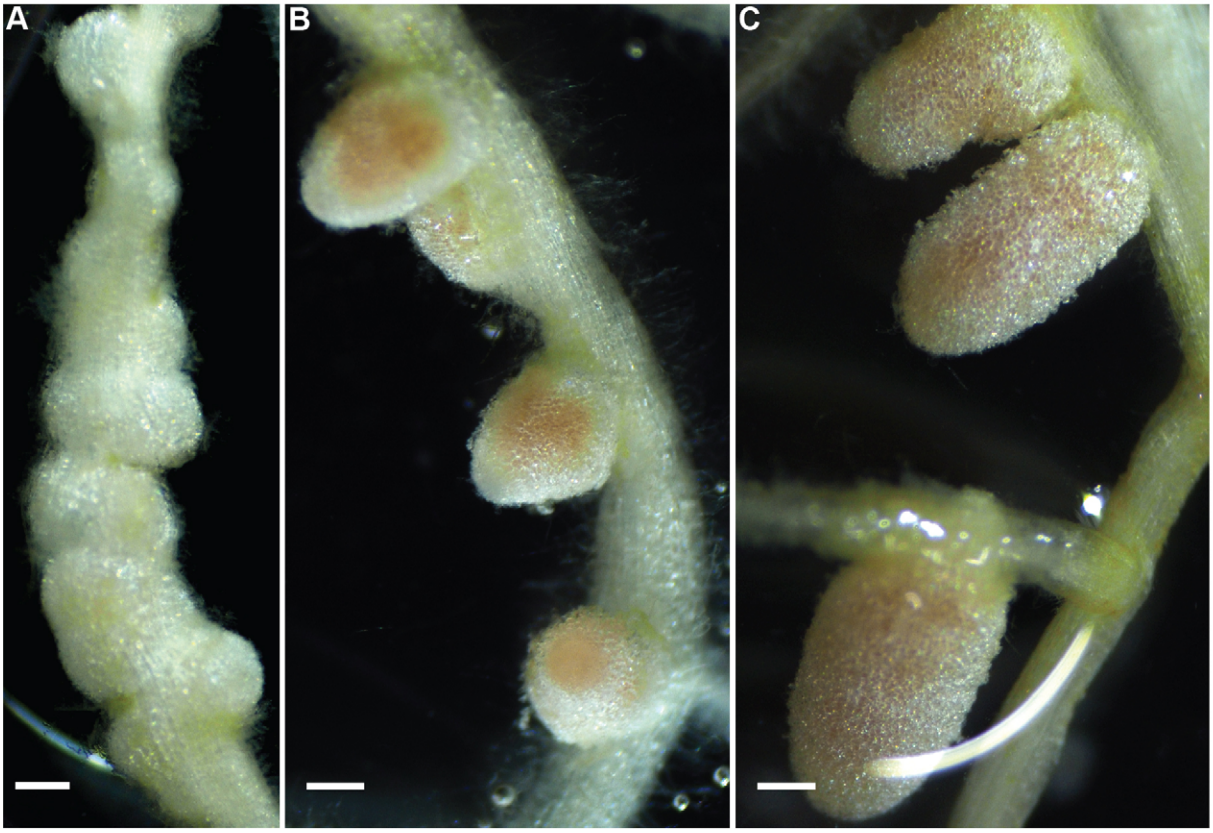

Fig. S4. Three weeks old *sickle* nodules (A-B) in comparison to wt nodules (C)

(A) Nodules formed at the "sickle" shaped zone. (B) Small pink nodules.

Bars, 250 μm.

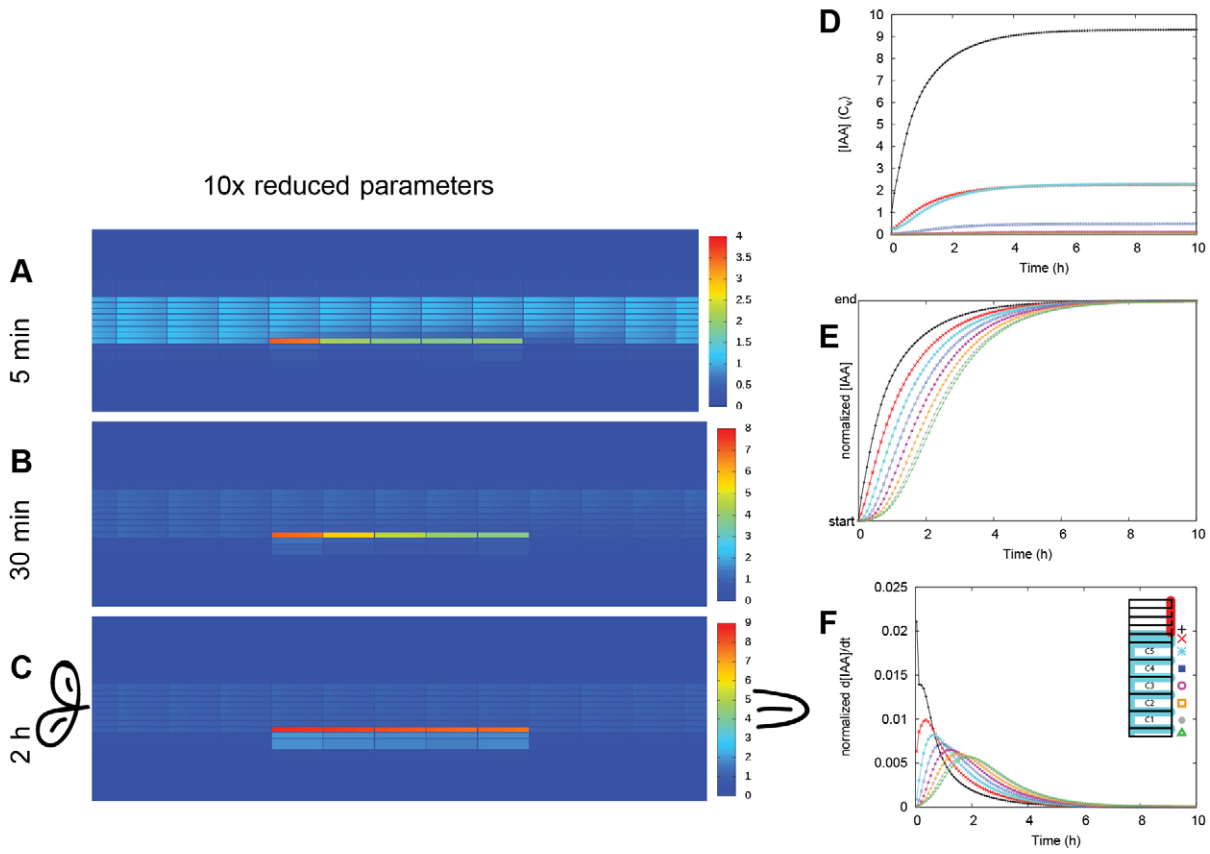

Fig. S5. Also with slowed down auxin dynamics, auxin accumulation following a local 10x reduction of the effective efflux permeability starts from the inner root layers.

The starting concentration of PINs in each membrane segment is one of three levels: "high" (red, P_{eff}=2 µm s^{-1}), "low" (cyan, P_{eff}=0.5 µm s^{-1}), or "bg" (white, P_{eff}=0.1 µm s^{-1}) (Deinum et. al, 2012). (A-C) Concentration heat maps of the part of the root segment including the controlled area at T=5 min (A), T=30 min (B) and T=2 h (C). (D) The concentration in the middle row of cells is tracked for all cell files in the controlled area. The concentration in the pericycle remains highest, followed by endodermis and inner cortex (C5). (E) When rescaling the concentration in each file from its starting level to the level reached at the end of the simulation (T=20 h), it becomes clear that the concentration in the pericycle increased first, followed by the other layers in an interior to exterior order. The moment of fastest concentration increase, the peaks of the curves in F (time derivative of E, expressed in rescaled concentration units per minute), showed the same relative order.

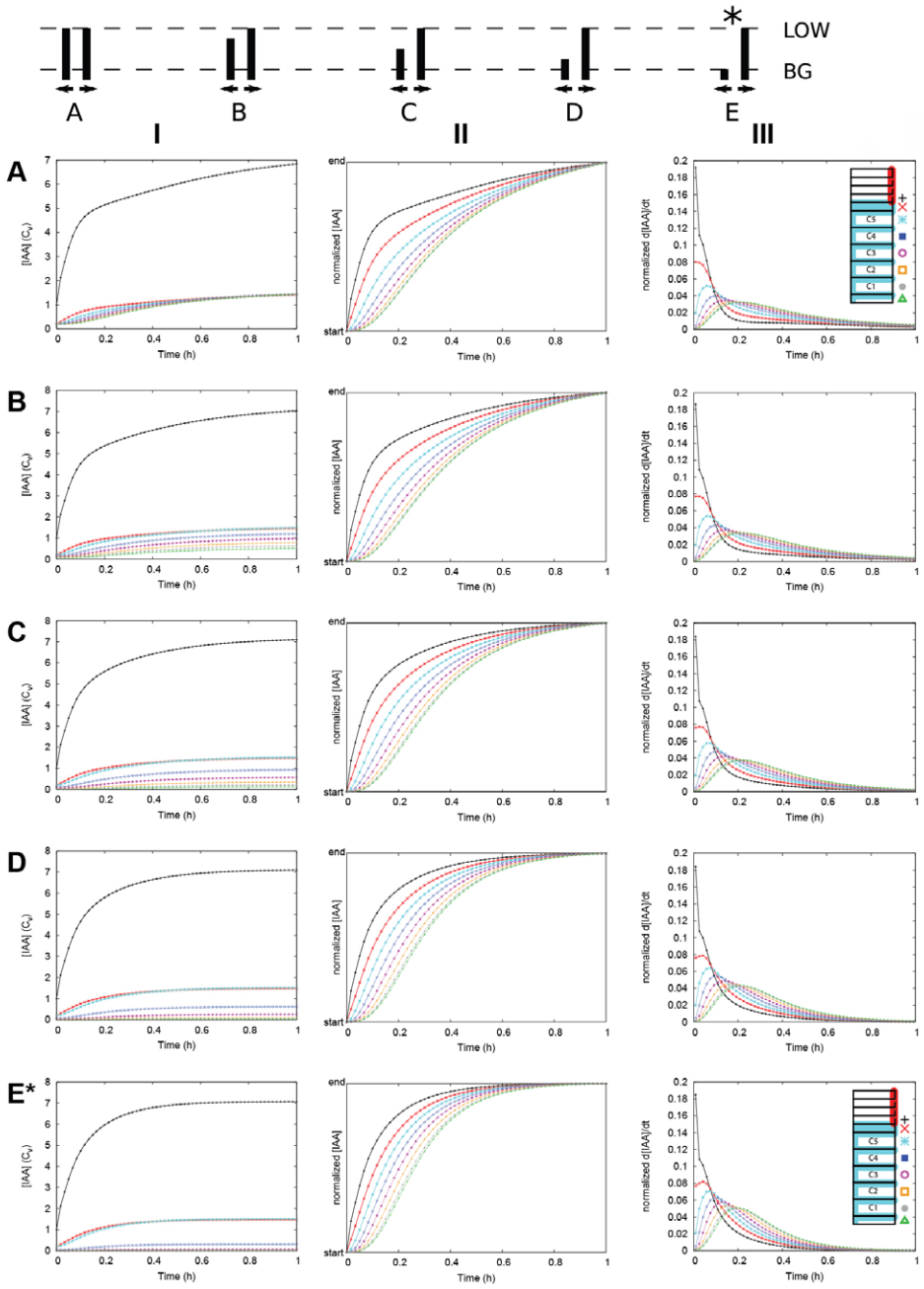

Fig. S6. Auxin accumulation always starts from the interior layers, regardless of inward: outward PIN bias in the cortex.

The amount of PIN (P_{eff}) before efflux reduction in the abaxial membrane of the cortical cells decreases from A, with P_{eff}=5 µm s^{-1} ("low") for abaxial and adaxial cell faces, to E, with P_{eff}=1 µm s^{-1} ("bg") for the abaxial cell face. This is illustrated in the cartoon on top. The root from Fig. 13, E in this figure, is marked with an asterisk (*). The full PIN distribution pattern is illustrated for A and E similar to Fig. 13B. This also shows the markers for the different cell layers. I: Concentration in the controlled area from the moment of efflux reduction (c.f. Fig. 13F). II: Concentration, rescaled from the initial value to the concentration at the end of the simulation (T=1 h; c.f. Fig. 13G). III: Concentration change. This is the time derivative of II, expressed in rescaled concentration units per minute (c.f. Fig. 13H). In all cases (A-E) the same relative order occurs: the first, strongest and fastest increase occurs in the pericycle, followed by endodermis, C5, etc. towards outer layers. The stronger the inward bias of the cortical PINs, the lower the steady state concentrations reached in the exterior root layers epidermis and outer cortex. It is likely that with a strong inward bias, i.e., towards the bottom of the figure, the maximum concentration reached in the outer cortex is insufficient to trigger a cell division response.

Movie 1. Concentration heat maps of the middle part of the root segment including the controlled area.